Boundary-Layer Meteorology (2025) 191:1
https://doi.org/10.1007/s10546-024-00890-w

RESEARCH ARTICLE

Momentum Transport in Heterogeneous Forest Canopies

Hawwa Kadum[1] · Ryan Scott[2] · Sarah E. Smith[2] · Marc Calaf[3] · Raúl Bayoán Cal[2]

Received: 8 April 2023 / Accepted: 24 October 2024
© The Author(s) 2024

Abstract
This study investigates the impact of spatial heterogeneity on momentum transport within forest canopies through wind tunnel experiments using 1:200 scale forest models. The models, crafted from 10 Pores Per Inch reticulated foam, emulate a leaf area index of 5.3 and include alternating patches and gaps of various sizes. Statistical results of the mean velocity profiles and velocity standard deviations show that the canopies develop a mixing layer. By employing lacunarity analysis to quantify spatial heterogeneity, we establish that the heterogeneity scale effectively represents variations in canopy height. The success of the lacunarity analysis as a metric is particularly noteworthy, providing a robust and practical measure of heterogeneity that can be easily applied in future research. Control volume analysis reveals that horizontal and vertical momentum advection terms rise as canopy heterogeneity increases, emphasizing its critical role in heterogeneous canopies and the possibility of describing this role using the lacunarity scale. The gaps also give rise to pressure terms through the local pressure gradient at each pattern. The study highlights the higher influence of gap size over heterogeneity scale on momentum flux. These insights contribute to improved parameterization of heterogeneous canopies in numerical weather prediction models, aiding in better representation of sub-grid scale processes and enhancing our understanding of canopy-atmosphere interactions.

Keywords Forest canopy · Lacunarity length scale · Momentum advection · Stereo particle image velocimetry (SPIV) · Surface heterogeneity

1 Introduction

The spatial heterogeneity of a surface alters the dynamics of the flow interacting with it (Pope 2000; Garratt 1978; Tajchman 1981; Poggi et al. 2004a; Avissar 1991). The interactions between these surfaces and the atmosphere control ecological, biological, and chemical processes occurring on the Earth's surface. Land surface properties such as topography, land use, soil type, soil moisture, and vegetation type vary on a spectrum of spatial and temporal scales. As a result, surface heterogeneity takes place at the same range of scales. Those sur-

✉ Hawwa Kadum
hawwa.kadum@kit.edu

[1] Institute for Meteorology and Climate Research-Atmospheric Environmental Research (IMKIFU/KIT), Garmisch-Partenkirchen, Germany

[2] Department of Mechanical and Materials Engineering, Portland State University, Portland, OR 97201, USA

[3] Department of Mechanical Engineering, University of Utah, Salt Lake City, UT 84112, USA

face properties are nonlinearly linked to the atmosphere through fluxes of energy, momentum, and mass (de Vrese et al. 2016; Sellers 1991). Even mild spatial variability in land surface properties can lead to significant changes in the exchange of energy, mass, and momentum in the atmospheric boundary layer (ABL) (Raupach and Finnigan 1997; Katul et al. 2006b). Understanding such processes becomes increasingly attractive to the scientific community with the increased interest in sustainable environmental practices and weather prediction enhancement (Garratt 1993; Wood 2000; Baldocchi et al. 2001).

Forest canopies cover vast areas of the Earth's surface and are highly heterogeneous. These canopies interact with the flow from scales as small as individual tree branches to gaps and patches on the order of the canopy boundary layer height. Plant canopy flows have been characterized by features that are different from a roughness boundary layer. Dense canopies boundary layer contain coherent turbulent eddies (Poggi et al. 2004b), gaps in energy cascades (Finnigan 2000), and a strong inflection point in the mean wind speed profile (Brunet 2020). These features have been explained by the mixing layer analogy (Raupach et al. 1996), however, the analogy is challenged when the canopy density is lower than a specific threshold (Brunet 2020). Many studies investigated the change in flow dynamics in relation to canopy density, but the change in gaps and horizontal distribution of the forest canopy, associated with density reduction, is not accounted for (Dupont and Brunet 2008; Huang et al. 2009). Latter studies show the dependency of flow dynamics on the horizontal structure of the canopy (Shig et al. 2023; Harman et al. 2016; Bailey and Stoll 2013; Bohrer et al. 2009; Schlegel et al. 2012). Changes in flow dynamics at the smallest scales within the forest canopy have been shown to affect larger scales above the canopy (Lo 1990; Finnigan 2000).

The challenges faced when dealing with surface heterogeneity can be divided into three main categories. First, surface heterogeneity occurs over a wide range of spatial scales ranging from millimeters to several kilometers (Bohrer et al. 2009; Finnigan 2000; Collins and Avissar 1994; Bou-Zeid et al. 2007). Therefore, it is challenging to characterize the heterogeneity impact on the ABL and to resolve all its scales in atmospheric simulations (Mahrt 2000; Bou-Zeid et al. 2020). Second, when the grid size used in the simulation domain is larger than the heterogeneity scales, the effects of these scales are not captured (Patton et al. 2005; Margairaz et al. 2020; Wyngaard 2004; Beare 2014). Lastly, there is no practical agreed upon method to measure heterogeneity which complicates efforts to obtain the relationship between level of heterogeneity and atmospheric processes. There have been efforts to overcome these challenges (Garratt 1990; Fontan et al. 2013). Previous research in this area studied the microscale effect of heterogeneity (Lopes et al. 2015; Bou-Zeid et al. 2007; Bohrer et al. 2009; Collins and Avissar 1994), momentum advection, dispersive stress, and secondary circulation (Rao et al. 1974; Higgins and Foley 2014; Raasch and Harbusch 2001; Ali et al. 2019; Viggiano et al. 2022), and developed models to parametrize the unresolved scale of surface variability (Bou-Zeid et al. 2020; Brunet 2020). However, two areas of development are still present. First, while research focus has been given to modeling the unresolved scales of heterogeneity in atmospheric models, the gap between models' predictions and observational data is still relatively large due to the models' inability to account for many small scale features like cumulus clouds, vegetation variability, and soil condition (Flato 2011). Hence, a more accurate representation of spatial heterogeneity is yet to be achieved. Second, to comprehensively characterize and model heterogeneity effect on ABL, this heterogeneity must be quantified first.

To achieve the aforementioned goals, wind tunnel experiments are conducted using an advanced forest canopy model developed specifically for this study. Reticulated foam cones mounted to wooden trunks were used in a canopy designed to accurately reflect momentum

and pressure losses for quantification of the shear stresses above the canopy (Gromke and Ruck 2018, 2008). The design of this canopy model marks a departure from previous models. The individual trees are based on geometric scaling to realistic trees. Furthermore, the canopy design is based on dynamic similarity in terms of Reynolds number rather than drag (Meroney 1968; Raupach et al. 1986; Lee and Lee 2012; Desmond et al. 2014; Stacey et al. 1994; Hamed et al. 2017; Raupach et al. 2006; Rodrigo et al. 2007). The design and scaling of the tree models are discussed in more detail in Sect. 3.1. Various forest canopy models composed of alternating patches and gaps are tested and compared to a uniform canopy. The gaps and patches introduce heterogeneity on various scales that allow examining the sub-grid scales of atmospheric models. The current work uses a single-valued heterogeneity parameter to quantify spatial heterogeneity. Thereafter, the implications of spatial heterogeneity on the canopy flow are investigated by studying the relation between heterogeneity parameter and momentum equation terms using control volume analysis (Cortina et al. 2016; Freedland et al. 2020; Stanislawski et al. 2020; De Roo and Mauder 2018).

The goals of this work are 1) Examining the interaction between the flow and a forest canopy using the new forest canopy model. 2) Quantify surface heterogeneity using a practical measure that can be easily obtained and used. 3) Describe how momentum transport terms change with surface heterogeneity, highlighting the relevance of the advection term. The theoretical framework for heterogeneity quantification and control volume analysis is outlined in Sect. 2. Details related to the experimental matrix, wind tunnel facility, and forest canopy elements are provided in Sect. 3. Results are presented in Sect. 4 starting with the development of a novel parameter designed to quantify spatial heterogeneity. The effectiveness of this parameter in characterizing momentum transport is determined through relevant mean flow statistics and bulk transport terms obtained from control volume analysis. Concluding remarks are given in Sect. 5.

2 Theory

2.1 Lacunarity

One challenge in studying the effect of surface heterogeneity on atmospheric processes is the lack of a practical metric that is able to reduce the complexity of heterogeneity accruing over a spectrum of scales as is the common case of Earth's surface properties. Lacunarity was initially proposed to measure the space filling nature of fractal patterns by Mandelbrot (1982). The concept was subsequently expanded to quantify general spatial heterogeneity in various deterministic datasets (Allain and Cloitre 1991; Plotnick et al. 1996; Kirkpatrick and Weishampel 2005). Since lacunarity reveals significant length scales, it has found application in numerous fields including the characterization of heterogeneous landscapes (Plotnick et al. 1993; Frazer et al. 2005; Kirkpatrick and Weishampel 2005).

Here, the lacunarity of each canopy arrangement is calculated via the gliding box algorithm developed by Plotnick et al. (1996). In the gliding box approach, a box is marked around a small portion of the domain occupied by elements starting at the origin of the domain. Then the mass density s of elements occupying this box of size B is determined, here it is the tree height at each spatial location. The box is moved across the domain to measure the mass density at different locations of the domain for the same box size. The box size is then increased in small increments to cover larger portions of the domain and the mass density at each box size is obtained using the same gliding box procedure. Large canopy composition

is often gathered via satellite images that provide $2D$ top view description. The images are then used to estimate canopy elements' height and density. For that reason, it is necessary to provide heterogeneity description for $2D$ surfaces. The method proposed by Frazer et al. (2005) was employed to produce one 2D plane of canopy heights and reduce mass density calculation time for each box. These mass density and box size results, whether obtained for $2D$ surfaces or $3D$ volumes, are then transformed into a probability distribution $Q(s, B)$ upon division by the total number of boxes. The Lacunarity is then defined as the ratio of distribution variance to its mean and is described as;

$$\text{Lacunarity(B)} = \frac{\sum s^2 Q(s, B)}{\left(\sum s Q(s, B)\right)^2} = \frac{s'^2(B)}{\overline{s}^2(B)} + 1, \tag{1}$$

where $\overline{s}$ represents the mean mass density and s' is the deviation from that mean.

Once the analysis covers all box sizes, a profile is obtained from the lacunarity value at each scale. Lacunarity profiles are classically used to gain information about spatial heterogeneity by highlighting various scales, the peak of the curve, the slope, and the lacunarity values. Given that heterogeneity can occur at multiple scales and is assessed through a probability function, it is useful to quantify this information through a single scalar value which can immediately indicate the heterogeneity of any canopy. In consequence, this proposed quantity encompasses all possible scales into a single quantity and opens the possibility of using this value to classify all types of heterogeneous surfaces.

The single quantity can be obtained by generalizing the lacunarity representation. First, we introduce here a new useful feature of those profiles, namely, the largest box size at which the lacunarity asymptotes. This size represents the scale after which there are no more spatial changes, see Scott et al. (2022) for details. Then, an analogy similar to the integral length scale taken in turbulent flows is made, where the area under the curve of normalized velocity correlations and length scales is integrated to determine the largest, most energetic turbulent scale in a particular flow (Pope 2000). Lacunarity profiles converge at different scales. These scales will be referred to as b and they always represent the largest spatial heterogeneity in a particular setup. The lacunarity profiles are then generalized by integrating over the relevant scales. The scale b is used to indicate the upper limit for integrating the lacunarity profiles to determine an integrated lacunarity length scale, L_c as,

$$L_c = \int_0^b \text{Lacunarity}\, dx. \tag{2}$$

This length scale is used to quantify spatial heterogeneity with a simple metric. The heterogeneity captured via L_c is solely geometrical making the approach practical and does not require complicated flow measurements. The influence of heterogeneity measured using this length scale is inspected by examining the momentum equation terms. The momentum equation theoretical description is presented in Sect. 2.2.

2.2 Reynolds Averaged Momentum Equation

The Reynolds averaged momentum equation is described as,

$$\frac{\partial u_i}{\partial t} + u_j \frac{\partial u_i}{\partial x_j} = -\frac{1}{\rho}\frac{\partial p}{\partial x_i} - \frac{\partial \overline{u_i' u_j'}}{\partial x_j} + \nu \frac{\partial^2 u_i}{\partial x_j^2} + f_i, \tag{3}$$

considering a steady high Reynolds number flow where viscous dissipation is negligible, the momentum equation reduces to:

$$u_j \frac{\partial u_i}{\partial x_j} + \frac{\partial \overline{u_i' u_j'}}{\partial x_j} = -\frac{1}{\rho}\frac{\partial p}{\partial x_i} + f_i, \tag{4}$$

where i & j indicates the coordinates x, y, and z. The bare variables are ensemble averaged, while variables with a prime represent temporal fluctuations. An overbar is used only to indicate an ensemble averaged covariance. For the streamwise momentum, the terms on the left hand side of the equation constitute the mean and turbulent momentum transport by advection and the shear stress, while the terms on the right hand side are the mean pressure gradient and the canopy mean drag force, respectively. The variables within these terms are ensemble averaged velocities, $u_{i,j}$, pressure, p, the drag force, f, and the density of air, ρ. Note that, although the index notation is used in this section, the symbols u, v, x, y, and z will be mainly used to indicate the streamwise velocity, vertical velocity, streamwise coordinate, vertical coordinate, and spanwise coordinate in other sections for simplicity.

To investigate the terms in Eq. 4 and their behavior under variant surface heterogeneity, we develop a control volume (CV) analysis of the different terms of the momentum equation. Evaluating the net momentum within the CV entails integrating every term in the equation over that CV as;

$$\overbrace{\iiint_v u_j \frac{\partial u_i}{\partial x_j} dv}^{\hat{A}} = -\overbrace{\iiint_v \frac{\partial \overline{u_i' u_j'}}{\partial x_j} dv}^{\hat{F}} + \overbrace{\iiint_v \Big[-\frac{1}{\rho}\frac{\partial p}{\partial x_i} + f_i \Big] dv}^{\hat{R}}, \tag{5}$$

where the volume integral of advection and shear stress terms are evaluated using surface integration by invoking the divergence theorem as follows,

$$\iiint_v u_j \frac{\partial u_i}{\partial x_j} dv = \sum_{n=1}^{6} \iint_{S_n} (u_i u_j) \cdot ni \; dS_n, \tag{6}$$

$$\iiint_v \frac{\partial \overline{u_i' u_j'}}{\partial x_j} dv = \sum_{n=1}^{6} \iint_{S_n} (\overline{u_i' u_j'}) \cdot ni \; dS_n. \tag{7}$$

After evaluating the surface integral over the six surfaces of the CV, the net value of each term is obtained. Control volume analysis provides information about the flow globally rather than locally. It captures the effects experienced by the flow field as a consequence of the flow coming in contact with the forest canopy and thus factors such as spatial heterogeneity can be evaluated taking into account all spatial variations. The advection and Reynolds shear stress gradient terms are calculated and the remaining terms including the local pressure term are grouped into a residual term and treated together. Note, the drag force f_i is zero in this investigation because the CV doesn't extend within the canopy as will be shown in the following sections. The residual term $\hat{R}$ is therefore obtained as $\hat{R} = \hat{A} - \hat{F}$.

3 Experimental Setup

The experiments proposed herein are designed to study the effects of heterogeneous forest canopy distribution on a turbulent boundary layer representative of the boundary layer of

a vegetated canopy. A heterogeneous forest canopy is represented as alternating patches of scaled model trees and gaps. Two different patch lengths and three different gaps are investigated as well as a homogeneous case with no gaps. The experiments are conducted in the Portland State University wind tunnel facility, and the data are collected via Stereo Particle Image Velocimetry (SPIV). Sections 3.1 and 3.2 present in detail the forest model and the experimental matrix.

3.1 Forest Model Description and Scaling

The model unit proposed here is a patch of inter-connected trees. Interactions between neighboring trees, such as branch meshing between two trees or more, introduce additional effects that necessitate the careful design of canopy models. By including neighbor interactions, models of averaged forest patches provide a realistic representation of canopy dynamics at the cost of neglecting individual tree characteristics (Rodrigo et al. 2007).

The tree model represents a conifer tree with a 200:1 scaling ratio. The model tree height $h_c = 10$ cm is divided equally into a 5 cm trunk and a 5 cm crown. The crown is a conical shape with a 44^o angle at the top and 4 cm diameter at the bottom. The tree trunk diameter is modeled according to the metabolic theory of ecology (MTE). The theory, introduced by West et al. (1999), employs the trees' stable metabolism to obtain an invariant morphological scaling between several tree dimensions including trunk diameter, branch diameter, tree height, crown area, and crown volume. The MTE is used in this work because it is species and age independent (Antin et al. 2013). Based on this, for a model crown diameter of 4 cm, a model trunk diameter is estimated to be 2 mm.

The patches are constructed with a reticulated foam that has a porosity of 10 PPI (Pore Per Inch). Reticulated foams have been shown to accurately reproduce flows within forest canopies (Gromke and Ruck 2018; Rodrigo et al. 2007). The foam porosity can be translated into a leaf area index (LAI) which is a measure of leaf to gap ratio per unit area. In this study, the LAI is obtained by taking images of the front view of a single tree placed in front of a white light source. The images are then processed to compute the ratio of black to white pixels. Black pixels represent areas covered with leaves, whereas white pixels represent the gaps. These ratios represent the leaf area density (LAD) at each vertical location. The LAI is then computed by integrating the LAD profile which is found to be 5.3 for the current tree model. Figure 1 shows the LAD profile of a single tree.

The canopy models are manufactured as patches. A sheet of reticulated foam with the desired dimensions of a single patch is soaked in coconut oil. This oil is chosen for its low solidifying temperature. The foam is then frozen to create a solid structure "mold" that can be machined. The mold is then machined with a high speed computer numerical control (CNC) machine using a cutting bit that is 44° angled to obtain the desired tree crown profile. While machining the foam, the produced trees are kept connected at the bottom. The patch is then washed to carefully remove the excess oil. Finally, the cut foam is placed on the tree trunks as shown in Fig. 2. Multiple patches are stacked together in order to create larger patches whenever needed.

3.2 Experimental Matrix

The experimental matrix is designed to investigate the effects of forest heterogeneity in the streamwise direction. The forest model consists of successive forest patches and gaps. The patch length (L_p) and the gap length (L_g) are determined according to the flow development

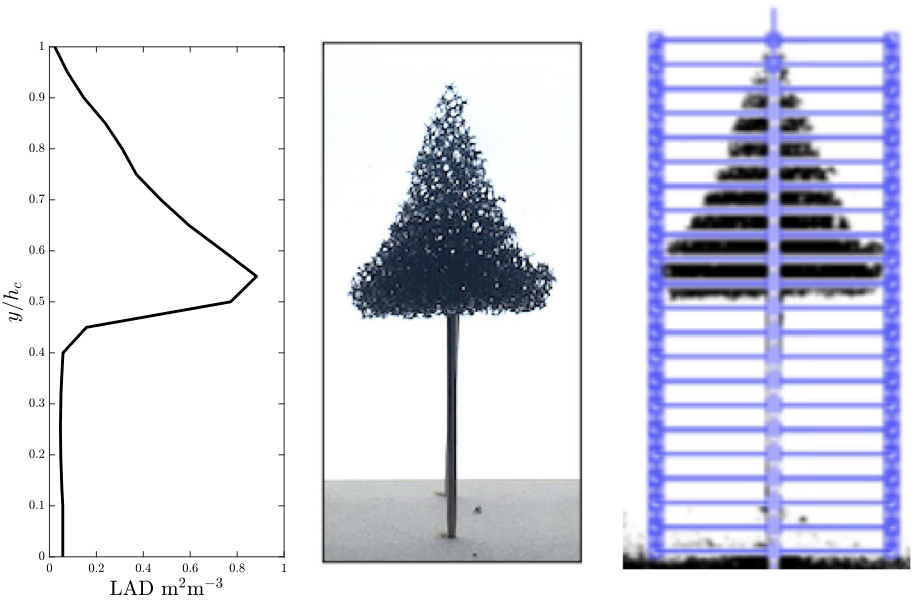

Fig. 1 From left to right, this figure presents a vertical profile of *LAD* of a single tree, an image taken for the front view of a tree with light source behind it, and the vertical segments over which the *LAD* is evaluated

Fig. 2 Forest patch model

within each patch as well as over the entire forest. Lopes et al. (2015) showed that the flow is fully developed when the number of forest patterns (forest patch followed by a gap) is at least 4. On this basis, the patch and gap lengths are chosen such that there are at least 4 patches upstream of the measurement location and one after it. The full matrix of proposed scenarios is presented in Table 1 along with the LAI, drag coefficient C_d, the friction velocity $u_\star$, and the heterogeneity scale L_c. The drag coefficient C_d is calculated from the momentum equation using vertical velocity profiles immediately behind the canopy similar to previous studies (Bitog et al. 2011). In the momentum equation, the advection, flux, and pressure terms are equal to the body force that is given as $[C_d\ a\ u^2]$, where a is the leaf area density integrated in the vertical direction. The resultant drag coefficient is also integrated in the vertical direction. The data collected in this study does not allow the computation of the pressure term, so the drag coefficient values here should be taken as a qualitative result, not quantitively. The friction velocity is calculated as $\sqrt{|\overline{u'v'}|_{h_c}}$.

Table 1 Matrix of patch and gap dimensions in terms of the model canopy height, $h_c = 10$ cm

Case	Patch length L_p	Gap length L_g	L_g/L_p	C_d	L_c (m)	$u_\star$(ms^{-1})	LAI
R_∞	$40h_c$	No Gap	0	NA	0.028	0.173	5.3
p_2g_1	$2h_c$	$1h_c$	0.5	0.98	0.13	0.197	
p_2g_2	$2h_c$	$2h_c$	1	0.85	0.16	0.200	
p_2g_4	$2h_c$	$4h_c$	2	0.54	0.2	0.223	
p_4g_4	$4h_c$	$4h_c$	1	0.8	0.3	0.234	

The table also presents the drag coefficient C_d and the geometrical heterogeneity scale L_c which will be discussed in later sections. The variable $u_\star$ is the friction velocity

3.3 Measurement Set 1: *xz* SPIV Planes

The experiments are conducted in a closed loop wind tunnel at the Portland State University facility, and the experimental setup is shown in Fig. 3. Stereo particle image velocimetry (SPIV) is used to take measurements in xz planes at five vertical locations, $y/h_c = 0.4, 0.75, 1.1, 1.25$, and 1.5. The SPIV measurement window is 20 cm $\times$ 20 cm which covers two canopy heights in either direction. The planes extend over a full pattern from the center of one patch to the center of a successive one. The measurements taken at heights below the canopy height cover only the gaps as it is not possible to collect measurements within the canopy, see Fig. 11 in the Appendix. Multiple successive SPIV planes are collected when the pattern length is longer than $2h_c$.

The number of snapshots collected for each case is 2500 at a frequency of 3.75 Hz. First and second order statistics convergence is tested to ensure a sufficient number of snapshots. For each measurement plane, the time difference between image pairs Δt is selected such that the maximum particle displacement in the measurement plane is 6 pixels. Data is collected at five vertical locations,and every time the laser sheet was moved to a new location, the cameras were moved accordingly to ensure that the same field of view area is covered. Collected images are processed using stereo cross correlation of 48 $\times$ 48 pixels interrogation area with 50% overlap followed by two passes of 24 $\times$ 24 pixels interrogation area. Erroneous vectors are removed using a median filter. Spurious vectors are replaced with vectors computed via interpolation from valid neighboring vectors. The uncertainty in the second order statistics was found to be 3% using the statistical correlation method implemented in DaVis version 8.4.0. based on (Wieneke 2015).

Three canopy-height based Reynolds numbers are tested using inflow velocities of 5 ms^{-1}, 7.5 ms^{-1}, and 10 ms^{-1} with an open tunnel arrangement. These velocities were chosen such that the corresponding Reynolds number exceeds the threshold for Reynolds number insensitivity of 50,000 established by Gromke and Ruck (2018) for two velocities. The 5 ms^{-1} inflow velocity was selected to provide information on the behavior of heterogeneous canopies under low speeds. An open tunnel arrangement was desirable as it allows the flow turbulence to be generated solely by the canopy. Forest models are placed at the tunnel entrance extending to the end of the test section to ensure measurements are recorded within the canopy boundary layer for all cases.

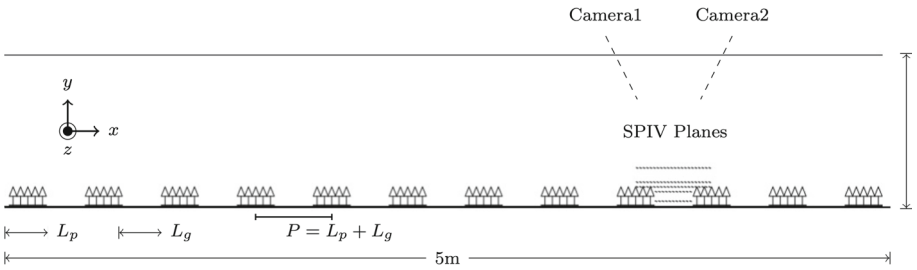

Fig. 3 Portland State University wind tunnel with model canopy patches and measurement planes to scale for $L_p = 2h_c$ and $L_g/L_p = 1$. Cameras' trajectories are not to scale

3.4 Measurement Set 2: *xy* SPIV Planes

The second set of measurements is collected for the same canopy arrangements introduced before, but the data is collected in an xy plane for vertical resolution. Two SPIV windows are stacked on top of each other vertically and collected simultaneously covering a distance of 40 cm from the tunnel floor, which is equivalent to $4h_c$. The measurements are taken in the gap between two successive patches. For cases where the gap size is larger than the SPIV window, two SPIV planes are collected in the streamwise direction to cover the entire gap. A broader range of inflow velocities are collected in this set of measurements including 1, 2, 5, 7.5, and 10 ms^{-1}.

Control volume analysis is applied to the upper and lower portions of the forest canopy separately. Separating the control volumes is intended to investigate the two layers of the canopy individually, namely the canopy layer ($1 \geq y/h_c > 0$, lower canopy hereafter) and the layer immediately above the canopy ($1.5 \geq y/h_c \geq 1$, upper canopy hereafter). The goal in considering each layer separately is to tie findings to their driving factors (patch length, gap length, and mean velocity forcing). Given the shared surface at canopy height y/h_c=1.1, these two control volumes are connected, and the exchanges occurring there are critical when evaluating heterogeneity; this will be demonstrated in the following sections. The xz measurement planes allow for this kind of partitioning due to the planes collected at different heights some within the lower canopy and some in the upper.

The upper canopy includes the flow above the canopy height. Three xz measurement planes taken at y/h_c=1.1, 1.25, and 1.5 are used to form the CV shown in Fig. 4. The lower canopy CV covers the gap between two patches in the streamwise direction and extends from y/h_c= 0.4 to y/h_c =1.1 vertically including measurement planes y/h_c=0.4, 0.75, and 1.1.

Linear interpolation is used to evaluate the vertical locations in-between the three planes. The interpolated data is validated by comparing the vertical profiles of first and second moment statistics to those obtained from the vertically resolved xy measurement plane. The profiles show good agreement, see Fig. 12 in the Appendix.

4 Results

4.1 Geometric Heterogeneity Quantification: Lacunarity Analysis

Figure 5 shows the lacunarity profiles for the forest canopy geometries tested in this study. Results demonstrate that for scales smaller than the tree crown diameter (indicated by a verti-

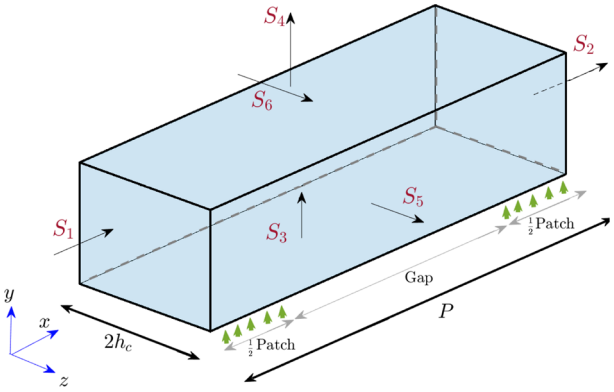

Fig. 4 Control volume schematic for the upper canopy. The CV covers a pattern distance P ($1/2L_p + L_g + \frac{1}{2}L_p$=$L_p$+ L_g) in the streamwise direction and extends from $y/h_c = 1.1$ to $y/h_c = 1.5$ in the vertical direction. The lower canopy CV is similar to this schematic except it covers only the gap region in the streamwise direction and extends from $y/h_c = 0.4$ to $y/h_c = 1.1$ vertically

cal dashed line), the profiles collapse for all cases. This is expected as the canopy arrangements have identical tree geometry as well as a uniform tree distribution. The differences between the study cases occur at larger scales represented by the gaps and patches. At scales larger than the crown diameter, the infinite canopy case R_∞ asymptotes because the canopy geometry is uniform and no changes occur when increasing the box size. The arrangements with larger gap sizes continue to develop as the box size increases further. Case p_2g_4 has the lowest tree density per pattern, hence its profile asymptotes at the lowest lacunarity value of 0.17. In contrast, case p_2g_1 converges at the highest lacunarity value of 0.34. The curves also extend over different box sizes before reaching the convergence scale (b). For the shorter pattern cases, as expected, all the spatial heterogeneity is contained within smaller box sizes. Case p_2g_1 converges at box size B=30 cm, while case p_4g_4 converges at box size B=80 cm. The box sizes required for each case to converge correspond to the pattern length. The convergence scale b is indicated by black arrows in Fig. 5 and its exact location on each lacunarity curve is marked with a star. This shows the richness of the lacunarity metric at providing a measure of the corresponding spatial variations.

4.2 Mean Velocity and Turbulence Quantities

Mean flow statistics are presented in Fig. 6 for the inflow velocity of u_∞= 7.5 ms^{-1}. The measurement planes cover only the gap length in the streamwise direction, and up to $4h_c$ in the vertical direction.

Streamwise velocity $\langle u/u_c \rangle$ profiles for the cases studied and from previous wind tunnel experiments are presented in Fig. 6a and b. The profiles display an inflection point as expected in a canopy flow similar to the profiles from the previous studies (Raupach et al. 1986; Brunet et al. 1994; Finnigan 2021). However, one can immediately notice the difference in velocity values between the present and previous studies. The current profiles have higher wind speeds above the canopy and reach the free-stream velocity at higher vertical locations. The main difference to keep in mind here is that the profiles in this work only cover the gap between two forest patches, while in previous studies they are either within the forest or immediately behind a single forest model. Other contributing factors to these differences are the patch's

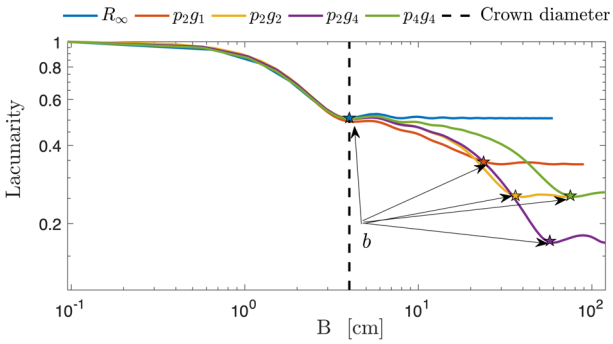

Fig. 5 Normalized $2D$ lacunarity profiles (shown in log scale) used to evaluate the lacunarity scale L_c for the canopy study cases. The curves are evaluated over 3 pattern lengths for each case to reach convergence. The dashed vertical line indicates the tree crown size and the black arrows point at the convergence scale (b) for each case shown as a star on each curve

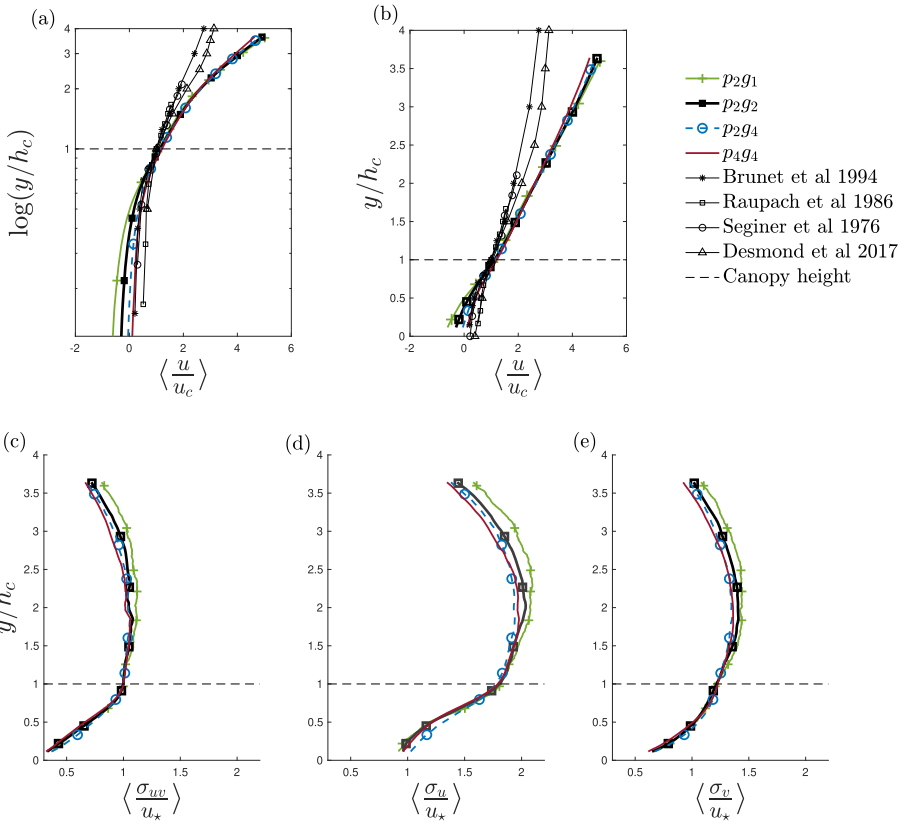

Fig. 6 Streamwise velocity component $\langle \frac{u}{u_c} \rangle$ and the normalized velocity standard deviations $\langle \frac{\sigma_{uv}}{u_\star} \rangle$, $\langle \frac{\sigma_u}{u_\star} \rangle$, and $\langle \frac{\sigma_v}{u_\star} \rangle$ for the various canopy arrangements averaged over the gap distance. Note that the x-axes are not the same for all subfigures. Inflow velocity $u_\infty = 7.5\,\mathrm{m\,s^{-1}}$

dense nature (LAI =5.3) and no gaps between the trees within the single forest patch (Brunet 2020; Finnigan 2000). The other difference is the profiles below the canopy. The current study profiles show a recirculation area (negative streamwise velocity). It can be seen in the averaged streamwise velocity profiles, Fig. 6a, of p_2g_1 and p_2g_2 due to their smaller gap size. When the gap size is small, the recirculation zone covers a larger area of the gap compared to bigger gap sizes, where the flow reattaches to the forest floor and recovers. Recirculation zones are common at patch exit when the patch density is high. This feature is related to the drag exerted by dense canopy composition.

Reynolds stress profiles averaged over the gap are shown in Fig. 6c, d, and e as velocity standard deviations, calculated as $\langle\sqrt{|\overline{u_i'u_j'}|}\rangle$, and normalized by the friction velocity, because the ratio between velocity standard deviations can indicate the boundary layer type developing above the canopy. Below the canopy, the shear increases with increased drag vertically. At canopy height, the standard deviations have the ratio of σ_{uv}: σ_u: σ_v = 1: 1.8: 1.22. They also show the $r_{uv} = \langle\overline{u'v'}\rangle/(\langle\sigma_u\rangle\langle\sigma_v\rangle) = -0.445$. These features in addition to the inflection point in the velocity profiles are indicators of the flow departing from an inertial sublayer behavior and displaying a mixing layer above the canopy gaps (Böhm et al. 2013). The mixing layer analogy was introduced by Raupach et al. (1996) where the authors suggested that the turbulent motion over a canopy is more pertinent to a mixing layer than a roughness layer. Having a fast moving flow above the canopy and a slow moving flow in the gap between two patches creates a mixing layer around the mixing plane (the canopy height). The turbulent eddies are less likely to penetrate dense canopies, nevertheless, having the gaps between patches in the current forest model allows the flow from above the canopy to enter the sub-canopy layer, hence generating mixing layer-like structures at the patch exit (Brunet 2020; Bailey and Stoll 2013). That said, mixing layers in canopies can have some differences from a plane mixing layer (Zhang et al. 2022; Bailey and Stoll 2016). The disposition of a canopy arrangement to develop a mixing layer depends highly on the canopy density and gap size. Having small gaps ensues a skimming flow regime where the bulk of the flow stays above the canopy and moves much slower than the flow higher than the canopy top leading to the formation of a mixing layer. For intermediate gap size, more flow can penetrate the gaps leading to the formation of a wake flow at one patch that interacts with the wake flow of another patch, creating a wake interference regime. This interaction creates regions of enhanced turbulence that contribute to developing a mixing layer as well. For larger gap sizes, turbulence is generated locally at the patch edge, but it is less likely to reach or interact with the turbulence generated by a successive patch. In that case, even though the canopy is fragmented, the flow resembles an isolated roughness flow regime in which a mixing layer is not probable (Oke 1988, 2002). Although the canopy gap sizes here fall into different flow categories presented in Oke (1988), the ratio of velocity standard deviations, the mean velocity inflection point, as well as the value of r_{uv} indicate that a mixing layer is indeed developed over all the cases studied. The flow regime limits in Oke (1988) are based on solid blocks, different from the porose tree-shaped models in this study.

Cassiani et al. (2008) reported a constant slope of shear stress decay to zero well above the canopy due to the canopy momentum absorption effect diminishing. The standard deviation profiles start decreasing steadily above $y/h_c = 2$. In case p_2g_1, shear stress decreases the slowest while cases p_2g_4 and p_4g_4 are the fastest. The shear stress does not vary significantly among the canopy arrangements. Similar trends are observed in the σ_u and σ_v profiles.

The results in this section show the general mean flow statistics for the gaps over different study cases. In the following sections, heterogeneity will be investigated using data that covers

the forest patches as well as the gaps through control volume analysis of the momentum equation.

4.3 Control Volume Analysis: Upper Canopy

The relation between canopy heterogeneity measured by the heterogeneity scale L_c and momentum transport terms is investigated herein. Figure 7 shows bar plots of the advection, Reynolds stress, and residual as defined earlier; each integrated over the various surfaces of the upper canopy CV. The terms are normalized by the canopy height and inflow velocity by multiplying them by (h_c/u_∞^2).

Figure 7a presents the surface integrated advection at each face of the CV for the upper canopy. Each surface contains five bars that correspond to the five canopy arrangements considered. The cases are organized on the $x-$axis in order of increasing heterogeneity scale from left to right. The coordinate system is illustrated in the schematic shown at the top of the figure. Positive and negative values of any quantity mean the momentum is transported in the positive or negative direction of the coordinate system. The streamwise advection in S_1 increases with increased heterogeneity. The two most heterogeneous cases L_c=0.2 and 0.3 ms correspond to cases p_2g_4 and p_4g_4, respectively. The two cases have similar gap sizes, but p_2g_4 has a smaller patch size that absorbs less momentum causing it to have higher streamwise advection. The advection leaving the CV through surface S_2 is of a similar magnitude for all cases to that entering through surface S_1. Surface S_3 of Fig. 7a shows an increase in vertical advection with heterogeneity at the canopy top ($y/h_c = 1.1$). It also shows a switch in the advection direction with larger gap sizes. The larger gaps cause an upward momentum advection near the canopy top. The mean flow is directed downwards when exiting a patch (Cassiani et al. 2008) leading to the flow being advected downwards starting at the canopy height. However, larger gaps allow the flow to recover downstream of the patch exit and generate an upwards flow near the next patch causing the upwards advection of the flow (Fontan et al. 2013). The effects of gap size and canopy density become less apparent higher up in the canopy as S_4 shows an increase in advection with heterogeneity and all cases are advecting momentum down into the canopy.

Figure 7b shows the turbulent flux through each surface. No significant dependence on the heterogeneity scale is observed in the streamwise component as shown through surfaces S_1 and S_2. The flux of momentum due to turbulence is relatively constant and is an order of magnitude smaller than that observed in the vertical direction (S_3 and S_4). In addition, the flux in the vertical direction in surface S_3 has a significant dependence on the heterogeneity scale. The flux $\hat{F}$ becomes more negative as the spatial heterogeneity is increased with p_4g_4 having the largest vertical flux - 4$\times$ larger than R_∞. The cause for this behavior is an increase in momentum transport into the canopy when the heterogeneity is increased since the flow is able to 'recover' over the larger patch and more intensely be driven downwards once the flow encounters the gap. This effect is present higher up in the canopy as can be seen from the identical behavior in surface S_4. The higher vertical fluxes are related to the sweep events Ali et al. (2017), and those are a feature of canopy flows. The sweep events take energy from the unobstructed flow above the canopy and move it downwards (Bailey and Stoll 2016).

The residual $\hat{R}$ is presented in Fig. 7c. The horizontal component is relatively large, but S_1 and S_2 are of similar magnitudes and nothing is added to the control volume. The vertical component, on the other hand, is not balanced. The vertical residual near the canopy height at S_3 is larger than that above the canopy at S_4. There is a source of residual in the control volume and that source value increases with heterogeneity scale. The flow over a canopy

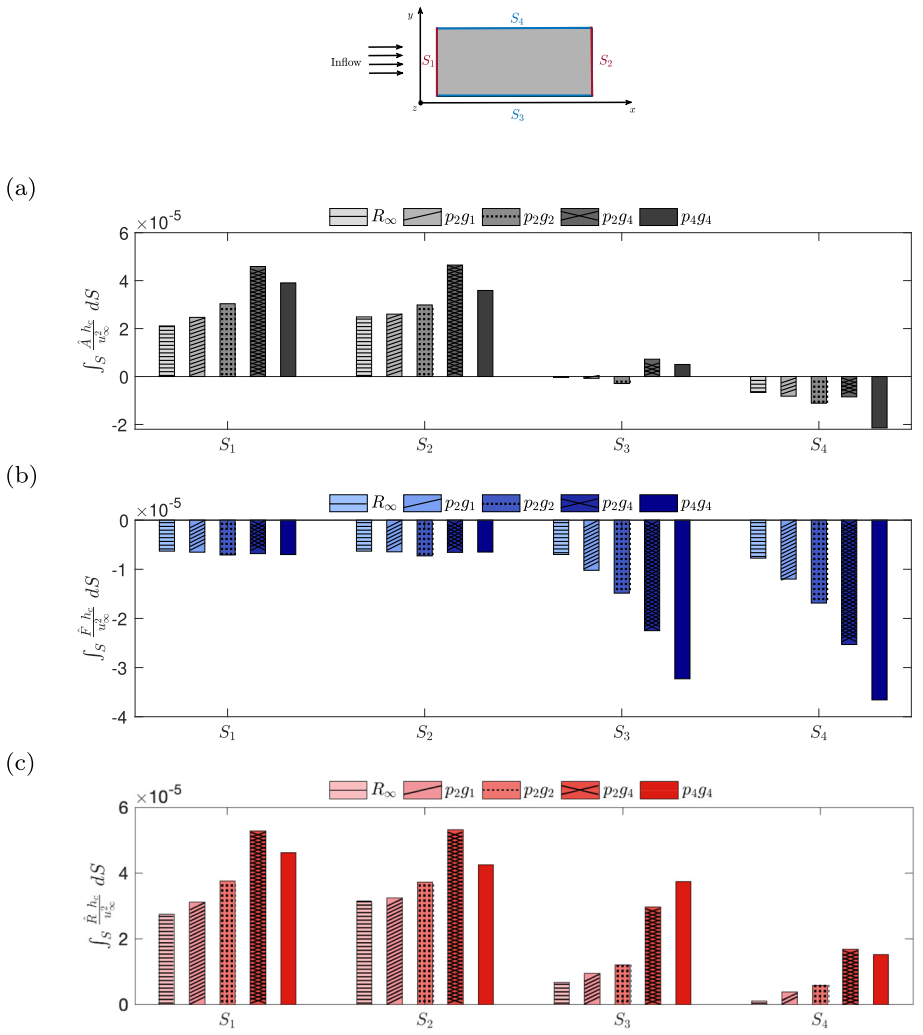

Fig. 7 Advection $\frac{\hat{A}\, h_c}{u_\infty^2}$ (**a**) Reynolds stress gradient $\frac{\hat{F}\, h_c}{u_\infty^2}$ (**b**) and residual $\frac{\hat{R}\, h_c}{u_\infty^2}$ (c) integrated over each surface for upper canopy plotted against heterogeneity scale L_c. Negative and positive values indicate momentum transport respectively in the negative and positive direction of the coordinate system illustrated in the schematic at the top of this figure

reaches equilibrium and fully develops after a certain distance downstream. However, with alternating gaps and patches the flow is always evolving (Poëtte et al. 2017). The canopy flow reaches a global equilibrium where the flow over one forest pattern is the same as over the next, but there is no local equilibrium. The flow is constantly developing over every single pattern once it reaches the patch where a local “internal boundary layer" develops over each pattern. When the flow above the canopy is fully developed " after 4 repeated “patterns", the internal boundary layers over all successive patterns are identical. The results for a control volume over one pattern represent the flow over any pattern at any streamwise location after the fourth pattern. See a schematic representation of the boundary layer in Fig. 13 in the Appendix. In

the current study, the measurement locations are within the developing boundary layer of the forest patterns. Meaning, the flow streamlines are still ascending vertically. The horizontal measurement planes will include horizontal and vertical components of the terms aligned with the boundary layer streamline. As a consequence, the residual term contributes to both vertical and horizontal components of the momentum. The increase is primarily through the canopy top at S_3, thus pointing towards the local pressure gradient in the streamwise direction and the momentum absorption by the canopy taking the primary role at the canopy height. Surface S_4 is significantly smaller in magnitude than in S_3 due to drag effects diminishing away from the canopy.

4.4 Control Volume Analysis: Lower Canopy

The surface integrated terms of the momentum equation in the lower canopy are shown in Fig. 8. The CV for the lower canopy covers only the gap in the streamwise direction and $y/h_c = 0.4$ to $y/h_c = 1.1$ in the vertical direction. Note here that the S_4 in the lower canopy is the same as S_3 in the upper canopy as both are located at $y/h_c = 1.1$. However, the quantities values are not the same because, in the upper canopy, S_3 extends to cover patches and gaps, while in the lower canopy, S_4 only covers the gap for consistency with the other measurement locations within the canopy sublayer where measurements inside the patches are not possible. The streamwise advection shown in Fig. 8 increases with heterogeneity in surface S_1, yet the effect of drag coefficient is observed in the sparse case p_2g_4 that shows the highest advection.

A significant difference in the vertical advection components is noted between surface S_3 and S_4. The vertical advection component is an order of magnitude lower than the horizontal advection component and it is almost negligible near the trunk layer in S_3. At the top lid, a downward advection is caused by the downward velocity motion at the forest gap exit. The advection in the lower canopy is lower than that in the upper canopy due to the flow being confined between two patches in the lower part of the canopy.

The Reynolds stress contribution in Fig. 8b shows that the streamwise component in S_1 is lower than the same component in S_2 which is a feature that did not occur in the upper canopy. The wall normal Reynolds shear stress component experiences a low shear region due to exiting a patch which is called a skimming flow regime (Hamed et al. 2020). In contrast, approaching a proceeding patch, the flow exhibits a shear layer growth regime (Hamed et al. 2020) where the turbulence increases and penetrates low in the canopy. These results are also in agreement with the study by Fontan et al. (2013). Those local differences in the lower canopy lead to its unique behavior compared to the upper canopy as well as among different canopy arrangements. The vertical component in S_3 and S_4 increases with heterogeneity showing a similar trend to the upper canopy, with the latter being higher in magnitude. The downward vertical flux is caused by sweep event dominance in canopy flows Bailey and Stoll (2016).

Finally, the residual term is shown in Fig. 8c. The streamwise component exhibits a similar trend in both S_1 and S_2. The two surfaces reflect the local effects of canopy arrangement on the advection and stress gradient terms. The difference between cases p_2p_4 and p_4g_4 is reduced in surface S_2 as the flow recovers downstream the patches compensating for any variation between the cases caused by their drag. The top surface S_4 shows the most variations among the study cases. The residual values are lower in this surface compared to S_3 as one would expect the largest drag force to be near the widest part of the tree foliage S_3, then decreases closer to the tree tops S_4 (Cassiani et al. 2008). The vertical

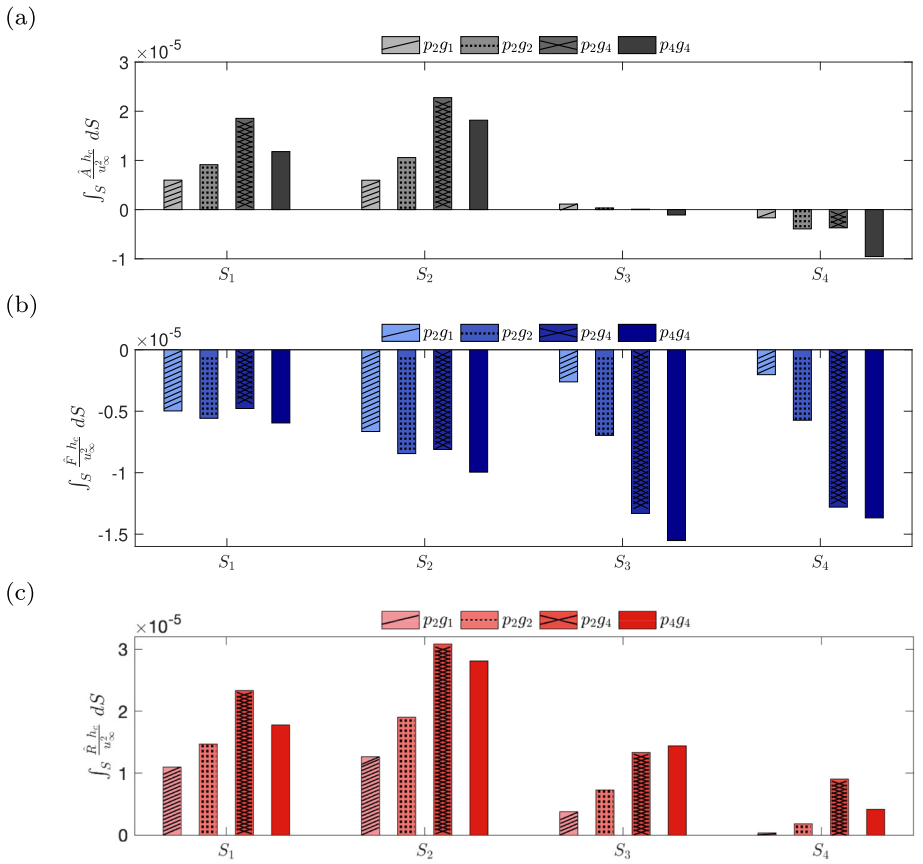

Fig. 8 Advection $\frac{\hat{A}\, h_c}{u_\infty^2}$ (**a**) Reynolds stress gradient $\frac{\hat{F}\, h_c}{u_\infty^2}$ (**b**) and residual $\frac{\hat{R}\, h_c}{u_\infty^2}$ (c) integrated over each surface for lower canopy plotted against heterogeneity scale L_c. Negative and positive values indicate momentum transport respectively in the negative and positive direction of the coordinate system illustrated in the schematic at the top of Fig. 7

and horizontal advection and residual values entering the control volume (CV) through S_1 and S_3 differ from those leaving through S_2 and S_4 due to heterogeneity perturbations. Theoretically, a homogeneous case should result in zero net momentum in each direction. However, in experimental setups involving multiple measurement planes, cameras, fields of view, and tunnel roof adjustments combined with data extrapolation, a certain percentage of error is inevitable, which can be seen in Fig. 9a where the homogeneous case has non-zero net horizontal and vertical advection. These errors will be addressed in the following results subsection by normalizing all heterogeneous cases against the homogeneous case. This normalization cancels out measurement uncertainty, ensuring that the results reflect solely the effects of alternating patches and gaps.

Figure 9 is a comparative plot of the contribution from horizontal and vertical advection to the total momentum advection in response to heterogeneity. The heterogeneity scale is normalized by canopy height h_c and von karman constant κ. When considering the canopy impact on the flow, a smaller advection leaving through S_2 than the advection entering through S_1 (i.e. S_1 - $S_2 > 0$) indicates that the canopy is a "sink" of advection. However, when

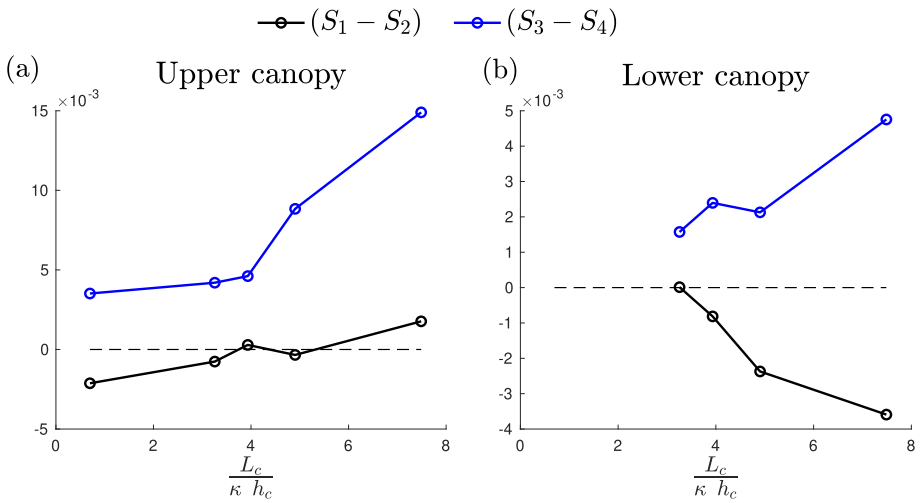

Fig. 9 The net horizontal $(S_1 - S_2)$ and vertical $(S_3 - S_4)$ advection in the upper and lower parts of the canopy. A positive quantity indicates a source of advection, while a negative quantity indicates a sink

discussing the contribution of advection to the momentum equation, a positive advection value represents a "source" of momentum. Hence, in this study, a positive quantity indicates a source of advection, while a negative quantity indicates a sink. In the lower canopy, Fig. 9b, the difference in magnitude between the vertical and horizontal components is not large and they are influenced equally by the heterogeneity as their values increase at a similar rate. The horizontal component is a sink of advection, while the vertical component is a source. The opposite signs of the two advection components are expected in canopies as demonstrated in the study by Katul et al. (2006a) on the effect of hilly terrains on Carbon Dioxide Exchange in a forest. In the upper canopy, the vertical component of advection is the main contributor being 3 times as large as the horizontal component. The vertical advection is always a source. The horizontal advection on the other hand is a sink in the lower heterogeneity cases. As the heterogeneity increases, this component shifts towards a neutral (almost zero contribution) in the intermediate cases before turning into a source in the most heterogeneous case $p_4 g_4$. The shift towards positive horizontal advection in the upper canopy here indicates the spatial heterogeneity influence in creating additional residual advection in the control volume.

4.5 Volume Integrated Momentum Transport Terms

The momentum equation terms are now integrated over the CV of each case for the upper and lower canopies. That is, the sum over all faces is undertaken as posed in Eq. 6 and Eq. 7. The trend each of these terms exhibits with heterogeneity is presented in Fig. 10. The advection and Reynolds stress are divided by a reference value $\hat{A}_\infty$ and $\hat{F}_\infty$ that correspond to the infinite canopy case R_∞.

Figure 10a shows how advection increases with the normalized heterogeneity scale $\frac{L_c}{\kappa\ h_c}$ in the upper canopy. The increase is significant and the increase in heterogeneity scale from $\frac{L_c}{\kappa\ h_c} = 0.7$ to $\frac{L_c}{\kappa\ h_c} = 7.5$ leads to increasing the advection in the upper canopy by a factor of 14 mainly due to the vertical component as discussed earlier in Fig. 9. The advection term behavior in the lower canopy is different from that in the upper canopy. In the lower

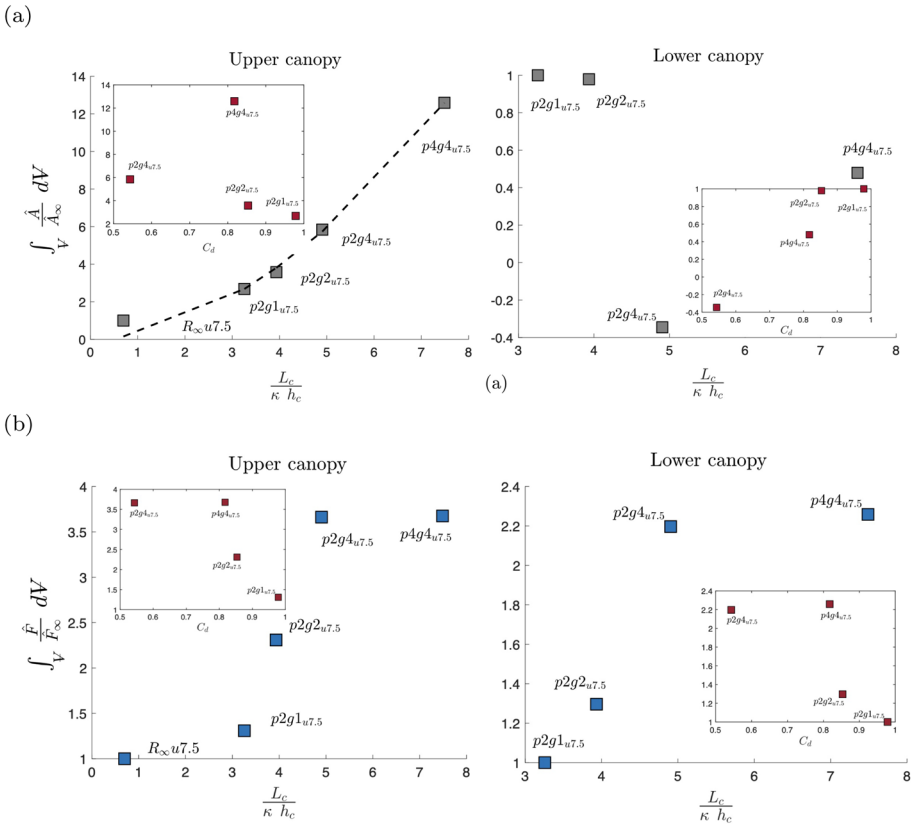

Fig. 10 Advection $\frac{\hat{A}}{\hat{A}_\infty}$ and Reynolds stress gradient $\frac{\hat{F}}{\hat{F}_\infty}$ integrated over the CV for upper and lower canopies. The upper canopy advection follows a power function of heterogeneity and the function is given by $(\frac{\hat{A}}{\hat{A}_\infty} = 1.64(\frac{L_c}{\kappa\ h_c})^{1.85})$. The terms are divided by a reference value $\hat{A}_\infty$ and $\hat{F}_\infty$ that is obtained from the reference canopy arrangement case R_∞. Arrangement p_2g_1 is considered as the reference case for the lower canopy

canopy, the advection decreases with increased heterogeneity scale, and no consistent trend is observed, especially for case p_2g_4. Case p_2g_4 is the most sparse arrangement, and it has the lowest patch to gap ratio and consequently, lower drag coefficient, see Table 1. The latter fact is demonstrated through the Advection-C_d plots (Maroon markers) superposed on the Advection-$\frac{L_c}{\kappa\ h_c}$ in Fig. 10a.

The integrated Reynolds flux gradient $\hat{F}$ is presented in Fig. 10b. The results show increasing Reynolds stress gradient values with higher $\frac{L_c}{\kappa\ h_c}$. An asymptotic behavior at higher heterogeneity values is observed. The heterogeneity scale increase from $\frac{L_c}{\kappa\ h_c} = 0.7$ to $\frac{L_c}{\kappa\ h_c} = 7.5$ results in a growth in the Reynolds stress divergence by a factor of 3.6 in the upper canopy. The stress gradient in the lower canopy responds to heterogeneity in a similar manner to the upper canopy and with the same order of magnitude. The similar behavior is also preserved in the turbulent flux-C_d plots superposed on the turbulent flux-$\frac{L_c}{\kappa\ h_c}$ plots. The fluxes decrease with increased drag in a similar manner to its increase with heterogeneity. This similarity suggests turbulence transport occurs as one process across the canopy layers

and it is gap size dependent. Canopies with larger gaps allow more of the upper flow to penetrate through the lower canopy creating turbulence exchange and mixing between the layers. Across-layer momentum exchange has important implications for forest growth, pollen dispersal, and water vapor and CO_2 cycles. It also shows that the canopy structure can alter the feedback between the canopy and the ABL. The results also highlight the importance of accounting for the advection term when investigating heterogeneous surfaces.

5 Conclusions

A set of forest canopy models is manufactured to emulate streamwise spatial heterogeneity by alternating patches and gaps. The heterogeneity scale L_c, based on lacunarity analysis, captured the heterogeneity successfully. Mean velocity and Reynolds shear stress profiles show the boundary layer above all the study cases is a mixing layer due to having both an inflection point as well as a ratio of σ_{uv}: σ_u: σ_v = 1: 1.8: 1.22. They also show the $r_{uv} = \langle\overline{u'v'}\rangle/(\langle\sigma_u\rangle\langle\sigma_v\rangle) = -0.445$. However, these results represent only the gaps between the forest patches, not the entire canopy pattern. The canopy structure of alternating gaps and patches creates a constantly evolving internal boundary layer over each forest pattern. These developing boundary layers lead to local pressure gradient formation even when the global flow is fully developed and in equilibrium. Hence, the study reports a non-zero vertical residual $\hat{R}$ and a non-zero horizontal advection component.

Control volume analysis of the momentum transport terms of the upper canopy highlights the significant influence of spatial heterogeneity on momentum advection (14 times increase when the heterogeneity scale increases from 0.028 to 0.3 ms in the current study). The vertical advection component is the primary contributor to the advection term and is a source, while the horizontal component is a sink. However, with increased heterogeneity, the horizontal component switches to a source leading to the increase in momentum advection in heterogeneous canopies. The turbulent flux is found to be affected by gap size rather than heterogeneity. **It is also found to exhibit similar behavior in both the upper and lower canopies.** Although the lower canopy shows less change in the magnitude of momentum transport terms with heterogeneity, it leads to much higher changes in the upper canopy flow and is also more influenced by the gap size.

The relation between heterogeneity parameters and momentum transport terms can serve as an addition to numerical weather prediction models representing scales smaller than their grid size. The heterogeneity scale can be used to represent the spatial variability within a single grid cell with relative ease as no flow parameters are needed in its estimation. The results showed a significant increase in momentum transport terms that should be taken into account when dealing with heterogeneous canopies. The results also highlight the significant role of mean flow in momentum transport when spatial heterogeneity is present.

Appendix

Figure 11 shows the mean streamwise velocity and the mean vertical velocity. The velocities are presented in all the horizontal measurement planes collected during the experiments.

In the control volume analysis, the horizontal planes in Fig. 11, for all the relevant variables, are integrated to obtain six surfaces of data. To check the accuracy of the integrated data, it was then averaged over area (only the gap area) and compared to the vertical profiles collected

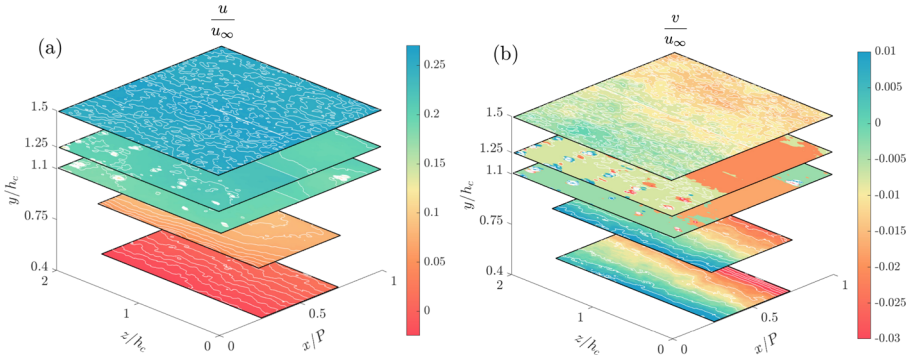

Fig. 11 Stack plot of the horizontal PIV planes collected for case p_2g_2 and inflow velocity 7.5 ms^{-1}. The streamwise velocity is in subplot (**a**) and the vertical velocity in subplot (**b**)

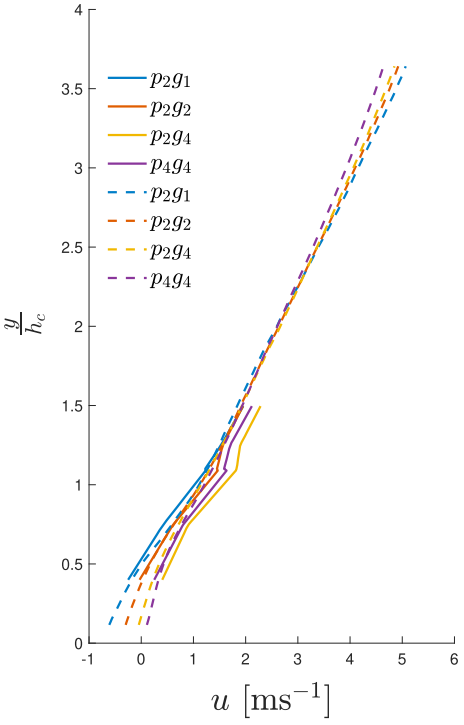

Fig. 12 Vertical profiles from 2D vertical PIV planes (dashed lines) vs. vertical profiles form the control volumes (solid lines) generated by integration of five horizontal planes shown in Fig. 11

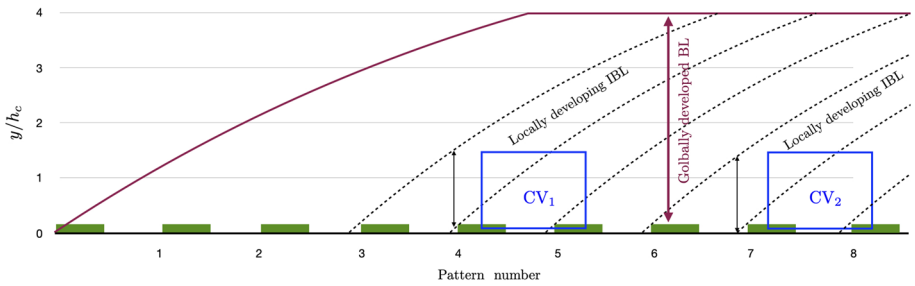

Fig. 13 A schematic showing the development of boundary layer over a canopy consisting of alternating patches and gaps. The figure shows the boundary layer is developed after four patterns in maroon. The dashed black lines represent the internal boundary layer (IBL) developed over each forest pattern. The blue boxes are control volumes containing an entire pattern in the streamwise directions. The flow inside CV_1 is identical to the flow inside CV_2. This state is referred to as "global equilibrium"

via the vertical PIV measurements detailed in Sec. 3.4. Figure 12 shows the good agreement between the vertical profiles of the streamwise velocity obtained from the integrated data and the vertical PIV planes.

Acknowledgements Raúl Bayoán Cal Cal acknowledges the National Science Foundation Grant (NFS-PDM-1712532). Marc Calaf acknowledges the National Science Foundation grant (NFS-PDM- 1712538).

Funding Open Access funding enabled and organized by Projekt DEAL.

Data Availability The datasets generated during and/or analyzed during the current study are available from the corresponding author on request.

Open Access This article is licensed under a Creative Commons Attribution 4.0 International License, which permits use, sharing, adaptation, distribution and reproduction in any medium or format, as long as you give appropriate credit to the original author(s) and the source, provide a link to the Creative Commons licence, and indicate if changes were made. The images or other third party material in this article are included in the article's Creative Commons licence, unless indicated otherwise in a credit line to the material. If material is not included in the article's Creative Commons licence and your intended use is not permitted by statutory regulation or exceeds the permitted use, you will need to obtain permission directly from the copyright holder. To view a copy of this licence, visit http://creativecommons.org/licenses/by/4.0/.

References

Ali N, Cortina G, Hamilton N, Calaf M, Cal R (2017) Turbulence characteristics of a thermally stratified wind turbine array boundary layer via proper orthogonal decomposition. J Fluid Mech 828:175–195

Ali N, Bossuyt J, Viggiano B, Ganapathisubramani B, Meyers J, Cal R (2019) Boundary layer development over a staggered multifractal roughness array. In: 11th international symposium on turbulence and shear flow phenomena, vol 30

Allain C, Cloitre M (1991) Characterizing the lacunarity of random and deterministic fractal sets. Phys Rev A 44(6):3552

Antin C, Pélissier R, Vincent G, Couteron P (2013) Crown allometries are less responsive than stem allometry to tree size and habitat variations in an indian monsoon forest. Trees 27(5):1485–1495

Avissar R (1991) A statistical-dynamical approach to parameterize subgrid-scale land-surface heterogeneity in climate models. Surv Geophys 12(1–3):155–178

Bailey BN, Stoll R (2013) Turbulence in sparse, organized vegetative canopies: a large-eddy simulation study. Boundary-Layer Meteorol 147(3):369–400

Bailey BN, Stoll R (2016) The creation and evolution of coherent structures in plant canopy flows and their role in turbulent transport. J Fluid Mech 789:425–460

Baldocchi D, Falge E, Gu L, Olson R, Hollinger D, Running S, Anthoni P, Bernhofer C, Davis K, Evans R et al (2001) Fluxnet: a new tool to study the temporal and spatial variability of ecosystem-scale carbon dioxide, water vapor, and energy flux densities. Bull Am Meteor Soc 82(11):2415–2434
Beare RJ (2014) A length scale defining partially-resolved boundary-layer turbulence simulations. Boundary-Layer Meteorol 151(1):39–55
Bitog J, Lee IB, Hwang HS, Shin MH, Hong SW, Seo IH, Mostafa E, Pang Z (2011) A wind tunnel study on aerodynamic porosity and windbreak drag. For Sci Technol 7(1):8–16
Böhm M, Finnigan JJ, Raupach MR, Hughes D (2013) Turbulence structure within and above a canopy of bluff elements. Boundary-Layer Meteorol 146(3):393–419
Bohrer G, Katul GG, Walko RL, Avissar R (2009) Exploring the effects of microscale structural heterogeneity of forest canopies using large-eddy simulations. Boundary-Layer Meteorol 132(3):351–382
Bou-Zeid E, Parlange MB, Meneveau C (2007) On the parameterization of surface roughness at regional scales. J Atmos Sci 64(1):216–227
Bou-Zeid E, Anderson W, Katul GG, Mahrt L (2020) The persistent challenge of surface heterogeneity in boundary-layer meteorology: a review. Boundary-Layer Meteorol 177(2):227–245
Brunet Y (2020) Turbulent flow in plant canopies: historical perspective and overview. Boundary-Layer Meteorol 177(2):315–364
Brunet Y, Finnigan J, Raupach M (1994) A wind tunnel study of air flow in waving wheat: single-point velocity statistics. Boundary-Layer Meteorol 70(1):95–132
Cassiani M, Katul G, Albertson J (2008) The effects of canopy leaf area index on airflow across forest edges: large-eddy simulation and analytical results. Boundary-Layer Meteorol 126(3):433–460
Collins DC, Avissar R (1994) An evaluation with the fourier amplitude sensitivity test (fast) of which land-surface parameters are of greatest importance in atmospheric modeling. J Clim 7(5):681–703
Cortina G, Calaf M, Cal RB (2016) Distribution of mean kinetic energy around an isolated wind turbine and a characteristic wind turbine of a very large wind farm. Phys Rev Fluids 1(7):074402
De Roo F, Mauder M (2018) The influence of idealized surface heterogeneity on virtual turbulent flux measurements. Atmos Chem Phys 18(7):5059–5074
Desmond CJ, Watson SJ, Aubrun S, Avila S, Hancock P, Sayer A (2014) A study on the inclusion of forest canopy morphology data in numerical simulations for the purpose of wind resource assessment. J Wind Eng Ind Aerodyn 126:24–37
de Vrese P, Schulz JP, Hagemann S (2016) On the representation of heterogeneity in land-surface-atmosphere coupling. Boundary-Layer Meteorol 160(1):157–183
Dupont S, Brunet Y (2008) Influence of foliar density profile on canopy flow: a large-eddy simulation study. Agric For Meteorol 148(6–7):976–990
Finnigan J (2000) Turbulence in plant canopies. Annu Rev Fluid Mech 32(1):519–571
Finnigan JJ (2021) The turbulent wind in plant and forest canopies. In: Plant disturbance ecology. Elsevier, pp 17–63
Flato GM (2011) Earth system models: an overview. Wiley Interdiscip Rev Clim Change 2(6):783–800
Fontan S, Katul G, Poggi D, Manes C, Ridolfi L (2013) Flume experiments on turbulent flows across gaps of permeable and impermeable boundaries. Boundary-Layer Meteorol 147(1):21–39
Frazer GW, Wulder MA, Niemann KO (2005) Simulation and quantification of the fine-scale spatial pattern and heterogeneity of forest canopy structure: a lacunarity-based method designed for analysis of continuous canopy heights. For Ecol Manage 214(1–3):65–90
Freedland GA, Eliason G, Solovitz S, Cal R (2020) The role of turbulent inflow on the development of a round jet in cross-flow. Int J Heat Fluid Flow 84(108):592
Garratt J (1978) Flux profile relations above tall vegetation. Q J R Meteorol Soc 104(439):199–211
Garratt J (1990) The internal boundary layer-a review. Boundary-Layer Meteorol 50(1):171–203
Garratt J (1993) Sensitivity of climate simulations to land-surface and atmospheric boundary-layer treatments-a review. J Clim 6(3):419–448
Gromke C, Ruck B (2008) Aerodynamic modelling of trees for small-scale wind tunnel studies. Forestry 81(3):243–258
Gromke C, Ruck B (2018) On wind forces in the forest-edge region during extreme-gust passages and their implications for damage patterns. Boundary-Layer Meteorol:1–20
Hamed A, Sadowski M, Nepf H, Chamorro L (2017) Impact of height heterogeneity on canopy turbulence. J Fluid Mech 813:1176–1196
Hamed AM, Peterlein AM, Speck I (2020) Characteristics of the turbulent flow within short canopy gaps. Phys Rev Fluids 5(12):123801
Harman IN, Böhm M, Finnigan JJ, Hughes D (2016) Spatial variability of the flow and turbulence within a model canopy. Boundary-Layer Meteorol 160:375–396

Higgins P, Foley A (2014) The evolution of offshore wind power in the united kingdom. Renew Sustain Energy Rev 37:599–612
Huang J, Cassiani M, Albertson J (2009) The effects of vegetation density on coherent turbulent structures within the canopy sublayer: a large-eddy simulation study. Boundary-Layer Meteorol 133(2):253–275
Katul G, Finnigan J, Poggi D, Leuning R, Belcher S (2006) The influence of hilly terrain on canopy-atmosphere carbon dioxide exchange. Boundary-Layer Meteorol 118:189–216
Katul G, Poggi D, Cava D, Finnigan J (2006) The relative importance of ejections and sweeps to momentum transfer in the atmospheric boundary layer. Boundary-Layer Meteorol 120(3):367–375
Kirkpatrick LA, Weishampel JF (2005) Quantifying spatial structure of volumetric neutral models. Ecol Model 186(3):312–325
Lee JP, Lee SJ (2012) Piv analysis on the shelter effect of a bank of real fir trees. J Wind Eng Ind Aerodyn 110:40–49
Lo AK (1990) On the determination of zero-plane displacement and roughness length for flow over forest canopies. Boundary-Layer Meteorol 51(3):255–268
Lopes AS, Palma J, Piomelli U (2015) On the determination of effective aerodynamic roughness of surfaces with vegetation patches. Boundary-Layer Meteorol 156:113–130
Mahrt L (2000) Surface heterogeneity and vertical structure of the boundary layer. Boundary-Layer Meteorol 96(1):33–62
Mandelbrot BB (1982) The fractal geometry of. Nature pp 394–397
Margairaz F, Pardyjak ER, Calaf M (2020) Surface thermal heterogeneities and the atmospheric boundary layer: the relevance of dispersive fluxes. Boundary-Layer Meteorol:1–27
Meroney RN (1968) Characteristics of wind and turbulence in and above model forests. J Appl Meteorol 7(5):780–788
Oke TR (1988) Street design and urban canopy layer climate. Energy Build 11(1–3):103–113
Oke TR (2002) Boundary layer climates. Routledge
Patton EG, Sullivan PP, Moeng CH (2005) The influence of idealized heterogeneity on wet and dry planetary boundary layers coupled to the land surface. J Atmos Sci 62(7):2078–2097
Plotnick RE, Gardner RH, O'Neill RV (1993) Lacunarity indices as measures of landscape texture. Landscape Ecol 8(3):201–211
Plotnick RE, Gardner RH, Hargrove WW, Prestegaard K, Perlmutter M (1996) Lacunarity analysis: a general technique for the analysis of spatial patterns. Phys Rev E 53(5):5461
Poëtte C, Gardiner B, Dupont S, Harman I, Böhm M, Finnigan J, Hughes D, Brunet Y (2017) The impact of landscape fragmentation on atmospheric flow: a wind-tunnel study. Boundary-Layer Meteorol 163(3):393–421
Poggi D, Katul G, Albertson J (2004) Momentum transfer and turbulent kinetic energy budgets within a dense model canopy. Boundary-Layer Meteorol 111(3):589–614
Poggi D, Porporato A, Ridolfi L, Albertson J, Katul G (2004) The effect of vegetation density on canopy sub-layer turbulence. Boundary-Layer Meteorol 111(3):565–587
Pope S (2000) Turbulent flows. Cambridge University Press
Raasch S, Harbusch G (2001) An analysis of secondary circulations and their effects caused by small-scale surface inhomogeneities using large-eddy simulation. Boundary-Layer Meteorol 101(1):31–59
Rao K, Wyngaard J, Coté O (1974) The structure of the two-dimensional internal boundary layer over a sudden change of surface roughness. J Atmosp Sci 31(3):738–746
Raupach M, Finnigan J (1997) The influence of topography on meteorogical variables and surface-atmosphere interactions. J Hydrol 190(3–4):182–213
Raupach M, Coppin P, Legg B (1986) Experiments on scalar dispersion within a model plant canopy part i: The turbulence structure. Boundary-Layer Meteorol 35(1–2):21–52
Raupach M, Finnigan J, Brunet Y (1996) Coherent eddies and turbulence in vegetation canopies: the mixing-layer analogy. In: Boundary-layer meteorology 25th anniversary, vol 1970–1995. Springer, pp 351–382
Raupach M, Hughes D, Cleugh H (2006) Momentum absorption in rough-wall boundary layers with sparse roughness elements in random and clustered distributions. Boundary-Layer Meteorol 120(2):201–218
Rodrigo JS, Van Beeck J, Dezsö-Weidinger G (2007) Wind tunnel simulation of the wind conditions inside bidimensional forest clear-cuts. application to wind turbine siting. J Wind Eng Ind Aerodyn 95(7):609–634
Schlegel F, Stiller J, Bienert A, Maas HG, Queck R, Bernhofer C (2012) Large-eddy simulation of inhomogeneous canopy flows using high resolution terrestrial laser scanning data. Boundary-Layer Meteorol 142(2):223–243
Scott R, Kadum H, Salmaso G, Calaf M, Cal RB (2022) A lacunarity-based index for spatial heterogeneity. Earth Space Sci 9(8):e2021EA002,180

Sellers P (1991) Modeling and observing land-surface-atmosphere interactions on large scales. In: Land surface-atmosphere interactions for climate modeling. Springer, pp 85–114
Shig L, Babin V, Shnapp R, Fattal E, Liberzon A, Bohbot-Raviv Y (2023) Flow and turbulence statistics of a two-height canopy model in a wind tunnel. Boundary-Layer Meteorol 187(3):591–617
Stacey G, Belcher R, Wood C, Gardiner B (1994) Wind flows and forces in a model spruce forest. Boundary-Layer Meteorol 69(3):311–334
Stanislawski B, Margairaz F, Cal R, Calaf M (2020) Potential of module arrangements to enhance convective cooling in solar photovoltaic arrays. Renew Energy
Tajchman SJ (1981) Comments on measuring turbulent exchange within and above forest canopy. Bull Am Meteor Soc 62(11):1550–1559
Viggiano B, Bossuyt J, Ali N, Meyers J, Cal RB (2022) Secondary motions above a staggered multi-scale rough wall. J Fluid Mech 941
West GB, Brown JH, Enquist BJ (1999) A general model for the structure and allometry of plant vascular systems. Nature 400(6745):664
Wieneke B (2015) Piv uncertainty quantification from correlation statistics. Meas Sci Technol 26(7):074002
Wood N (2000) Wind flow over complex terrain: a historical perspective and the prospect for large-eddy modelling. Boundary-Layer Meteorol 96(1):11–32
Wyngaard JC (2004) Toward numerical modeling in the "terra incognita". J Atmos Sci 61(14):1816–1826
Zhang W, Zhu X, Yang XI, Wan M (2022) Evidence for raupach et al.' mixing-layer analogy in deep homogeneous urban-canopy flows. J Fluid Mech 944:A46

Publisher's Note Springer Nature remains neutral with regard to jurisdictional claims in published maps and institutional affiliations.